Electronic Supplementary Material (ESI) for Nanoscale.
This journal is © The Royal Society of Chemistry 2022

MBE-Grown Ultrathin $PtTe_2$ Film and the Layer-Dependent Electronic Structure

Lei Zhang,[a,b] *Tong Yang,*[c] *Arramel,*[b,d] *Yuan Ping Feng,*[b,e] *Andrew T. S. Wee*[b,e] *and Zhuo Wang,*[*a]

[a]SZU-NUS Collaborative Innovation Center for Optoelectronic Science & Technology, International Collaborative Laboratory of 2D Materials for Optoelectronics Science and Technology of Ministry of Education, Institute of Microscale Optoelectronics, Shenzhen University, Shenzhen 518060, China.

[b]Department of Physics, National University of Singapore, 2 Science Drive 3, Singapore 117551, Singapore

[c]Department of Applied Physics, The Hong Kong Polytechnic University, Hung Hom, Hong Kong SAR, China

[d]Nano Center Indonesia, Jl. PUSPIPTEK Tangerang Selatan, Banten 15314, Indonesia

[e]Centre for Advanced 2D Materials (CA2DM) and Graphene Research Centre (GRC), National University of Singapore, 6 Science Drive 2, Singapore 117546, Singapore

Corresponding author: Zhuo Wang (wzhuo@szu.edu.cn)

1. Raman spectrum of the sample grown at 500 ℃

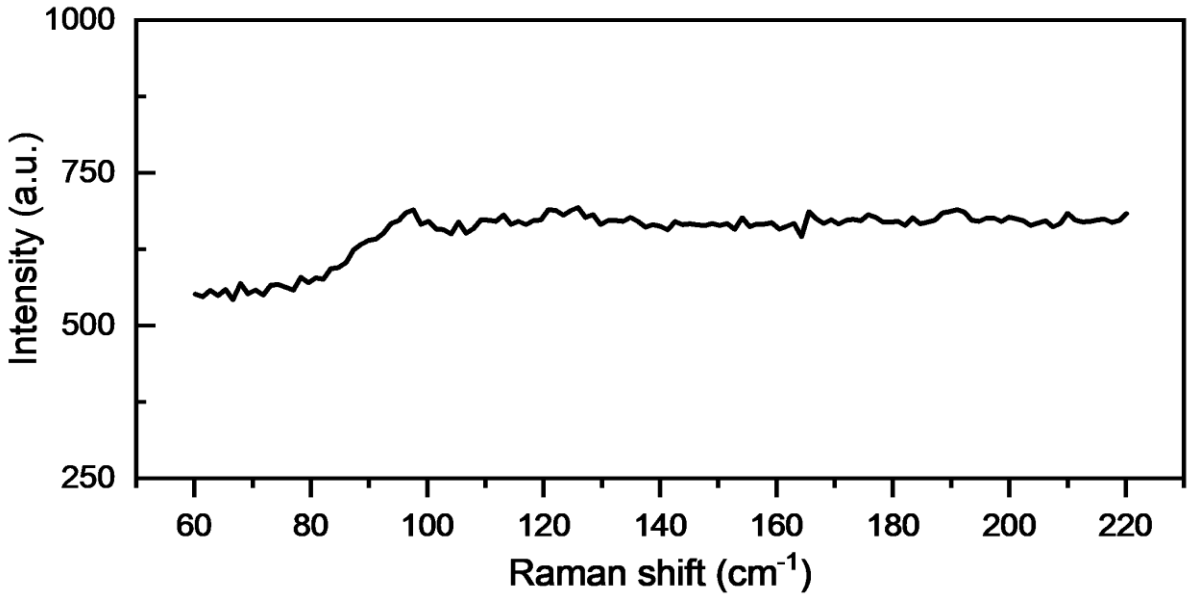

Figure S1. Raman spectrum of the sample corresponding to Figure 4d showing no obvious characteristic peaks of 2D $PtTe_2$.

2. Determination of the bandgap of monolayer $PtTe_2$

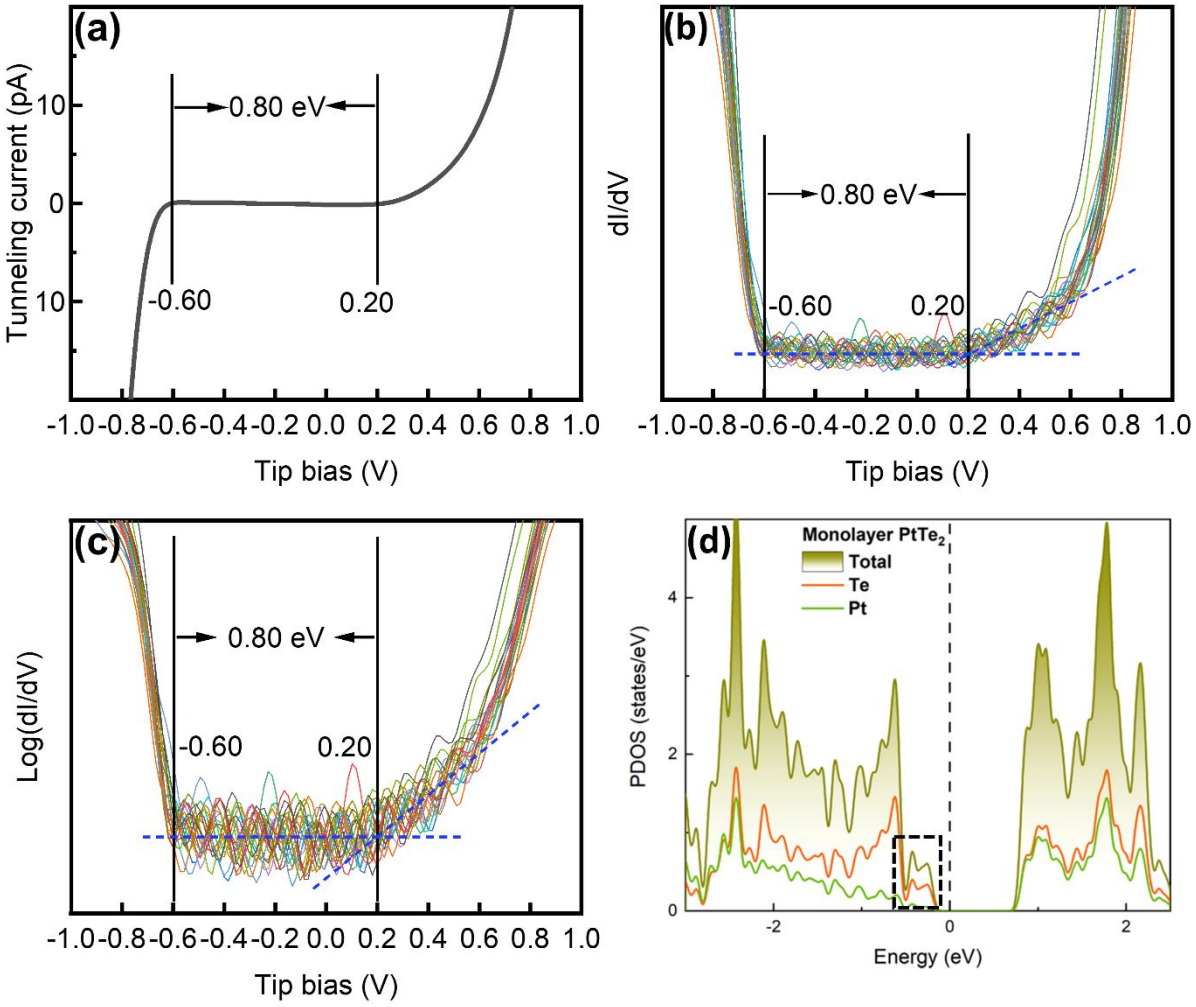

Figure S2. (a) Tunnelling current *vs* Tip bias curve. (b) dI/dV *vs* Tip bias curve. (c) Log(dI/dV) *vs* Tip bias curve for better identification of the bandgap. (d) The HSE06 projected density of states (PDOS) of monolayer $PtTe_2$. The curve in (a) is the averaged tunnelling current of 20 STS scans. (b) and (c) are the curves of the same group of STS scans.

The determination of the bandgap of monolayer $PtTe_2$ takes into account the (a) I-V, (b) dI/dV and (c) Log(dI/dV) curves. By zooming in the vertical axis of I-V curve (Figure S2a), it can be seen that the tunnelling current remains zero in the tip bias range from –0.60 to 0.20 V and starts rising up out of this bias range. The bandgap is bettered identified by the zoomed-in dI/dV (Figure S2b) and Log(dI/dV) (Figure S2c) curves. Apparently, in the negative tip bias range the curves start rising up at –0.60 V, which means the conduction band minimum (CBM) is located at 0.60 eV above the Fermi level. In the positive tip bias range, the rising-up position is not as obvious as that in the negative bias

range. This is because the density of states (DOS) is much smaller near the valence band maximum (VBM), as indicated by our DFT calculations (the black dotted square in Figure S2d). To bettered identify the VBM position, we zoomed in very much the curves in Figure S2b and c. It can be seen that the flat part and the sloped part intersect at 0.20 eV, which is the same as the rising position of tunnelling current shown in Figure S2a. Therefore, the VBM is determined to be at 0.20 eV below the Fermi level. Based on more than two hundred STS on different crystal islands of different samples, the error of the bandgap is determined to be ± 0.05 eV. Hence, the bandgap of monolayer $PtTe_2$ is 0.80 ± 0.05 eV.

3. DFT calculation details

Table S1. The interlayer binding energy density of the nth $PtTe_2$ layer with the (n-1)-layer $PtTe_2$ supported on graphene (ε_n). The binding energy density of graphite and bulk $PtTe_2$ are also listed. It is noted that our calculated interlayer binding energy density of graphite is very similar to that determined experimentally.

$\boldsymbol{\varepsilon_1}$	–17.6 meV/Å^2
$\boldsymbol{\varepsilon_2}$	–28.8 meV/Å^2
$\boldsymbol{\varepsilon_3}$	–29.0 meV/Å^2
$\boldsymbol{\varepsilon_4}$	–30.5 meV/Å^2
Bulk $PtTe_2$	–30.4 meV/Å^2
Graphite	–26.6 meV/Å^2 (equivalent to –35.0 meV/atom)
Graphite [Ref. 1]	–31±2 meV/atom

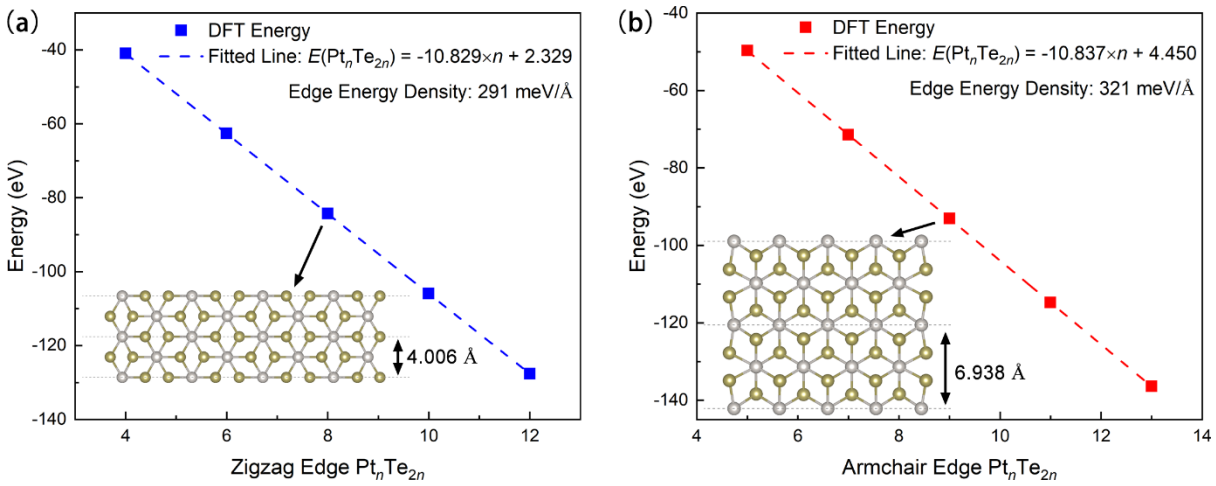

Figure S3. The total energy of the $PtTe_2$ nanoribbons with the (a) zigzag and (b) armchair edge as a function of the number of formula units (Pt_nTe_{2n}). The inset shows the adopted model at $n = 8$ in (a) and 9 in (b). The linear line fitted to the DFT energies is shown and the extrapolated edge energy density is marked as well in both panels.

The energy density of $PtTe_2$ edges (γ) can be calculated by the extrapolation of the DFT-calculated total energy of $PtTe_2$ nanoribbons. Herein, $PtTe_2$ nanoribbons were constructed with both edges being either zigzag or armchair. The width of the nanoribbon was further varied, which can be measured by the number of formula units of $PtTe_2$ contained in the model (n), *i.e.*, Pt_nTe_{2n}. The insets of Figure S1 show the adopted Pt_nTe_{2n} nanoribbons with the zigzag edge at $n = 8$ and the armchair edge at $n = 9$. The total energy of a Pt_nTe_{2n} nanoribbon comprises both the bulk and the edge contributions, which can be written as:

$$E(\mathrm{Pt}_n\mathrm{Te}_{2n}) = a \times n + 2 \times L \times \gamma$$

where slope a is the energy per formula unit of bulk $PtTe_2$. 2 accounts for the two identical edges and L denotes the lattice constant along the edge (4.006 Å along the zigzag edge and 6.938 Å along the armchair edge). As shown in Figure S1, the DFT-calculated total energies can be well fitted for both zigzag and armchair nanoribbons, which gives the edge energy density of γ =291 meV/Å and 321 meV/Å for the zigzag and armchair edge, respectively. Therefore, the more stable zigzag edge will be considered for analysing the competition between the interlayer-binding-induced energy lowering and edge-formation-induced energy increase in the main text.

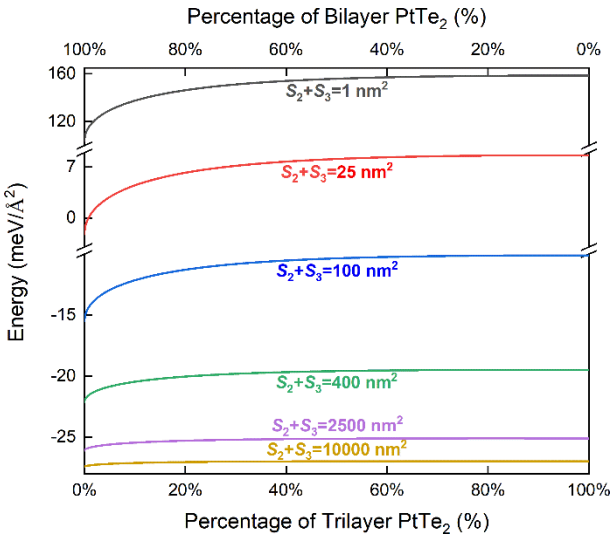

Figure S4. The total energy per unit area (E) of a $PtTe_2$ island as a function of the area percentage of bilayer/trilayer $PtTe_2$ at a given total area of the second and third $PtTe_2$ layers ($S_2 + S_3$). The total area ranges from 1 to 10000 nm^2. It is assumed that the first $PtTe_2$ layer is large enough to support the growth of the second and third $PtTe_2$ layers, and the energy contribution from the first layer is omitted.

References:

Liu, Ze, et al. "Interlayer binding energy of graphite: A mesoscopic determination from deformation." *Physical Review B* 85.20 (2012): 205418.